



Design and Synthesis of a Biochar-Supported Nano Manganese Dioxide Composite for Antibiotics Removal From Aqueous Solution

Jiang Li¹, Xiaoxi Cai^{2*}, Yunguo Liu³, Yanling Gu⁴, Hui Wang⁵, Shaobo Liu¹, Simian Liu¹, Yicheng Yin³ and Sijia Liu³

¹ School of Architecture and Art, Central South University, Changsha, China, ² College of Art and Design, Hunan First Normal University, Changsha, China, ³ College of Environmental Science and Engineering, Hunan University, Changsha, China, ⁴ College of Materials Science and Engineering, Changsha University of Science and Technology, Changsha, China, ⁵ College of Environmental Science and Engineering, Central South University of Forestry and Technology, Changsha, China

OPEN ACCESS

Edited by:

Baharak Sajjadi,
University of Mississippi,
United States

Reviewed by:

Isaac Dennis Amoah,
Durban University of Technology,
South Africa
Zacharias Frontistis,
University of Western Macedonia,
Greece

*Correspondence:

Xiaoxi Cai
xiaoxi@hnu.edu.cn

Specialty section:

This article was submitted to
Water and Wastewater Management,
a section of the journal
Frontiers in Environmental Science

Received: 04 March 2020

Accepted: 01 May 2020

Published: 22 May 2020

Citation:

Li J, Cai X, Liu Y, Gu Y, Wang H,
Liu S, Liu S, Yin Y and Liu S (2020)
Design and Synthesis of a
Biochar-Supported Nano Manganese
Dioxide Composite for Antibiotics
Removal From Aqueous Solution.
Front. Environ. Sci. 8:62.
doi: 10.3389/fenvs.2020.00062

Manganese dioxide nanoparticles were loaded onto biochar prepared from rice husk to obtain a biochar-supported manganese dioxide composite (BC/MnO₂). The properties of this composite were studied through various advanced characterization techniques, combined with experiments on treating aqueous solutions of tetracycline hydrochloride (TC) and doxycycline (DC). The results showed that compared with the original biochar, MnO₂ nanoparticles appeared on the surface of BC/MnO₂, the carbon content decreased, and the oxygen content increased. Moreover, BC/MnO₂ exhibited significantly larger total pore volume and specific surface area, and the pore structure of the biochar was improved. The effect of pH on the adsorption of TC and DC by BC/MnO₂ was insignificant. With an increase in the adsorbent dose, the removal rates of TC and DC increased, and the removal ability of BC/MnO₂ for TC was slightly higher than that for DC. The adsorption of TC and DC on the BC/MnO₂ surface conformed to the Freundlich model. Compared with the pseudo-first-order kinetic model, the pseudo-second-order kinetic model ($R^2 = 0.999$) better fitted the adsorption data, indicating that the adsorption process is controlled by chemical adsorption. In addition, the results of adsorption-desorption experiments indicated that BC/MnO₂ have excellent regeneration ability. The experimental results of this study are significant for expanding the application of biochar composites in the treatment of aqueous solution containing antibiotics.

Keywords: biochar, composite, adsorption, tetracycline hydrochloride, doxycycline

INTRODUCTION

Antibiotics are widely used for preventing bacterial infections in humans and animals (Luo et al., 2011; Hong et al., 2013). Since the discovery of antibiotics, their global production and use have been increasing rapidly, causing some concern (Kasprzyk-Hordern et al., 2009). Antibiotics have different half-lives in the environment, and some of them have high persistence; therefore, they have been polluting the environment at an alarming rate (Petrie et al., 2015; Carvalho and Santos, 2016).

Abbreviations: BC/MnO₂, Biochar-supported manganese dioxide composite; BET, Brunner-Emmett-Teller; DC, Doxycycline; FTIR, Fourier transform infrared spectroscopy; SEM, Scanning electron microscopy; TC, Tetracycline hydrochloride; TG, Thermogravimetric; XPS, X-ray photoelectron spectroscopy.

Residues have been frequently detected in surface water and groundwater worldwide (Homem and Santos, 2011; Yu et al., 2016). Notably, long-term exposure to antibiotic residues at relatively low concentrations can induce antibiotic resistance genes (Ahmed et al., 2015; Huang et al., 2015; Hou et al., 2016; Sharma et al., 2016). Due to the exposure to sublethal concentrations of antibiotic residues, drug-resistant strains of pathogens have become the dominant strains, which have rapidly developed and inherited antibiotic resistance genes. Therefore, antibiotics are ineffective against the pathogens with the corresponding antibiotic resistance genes, rendering their infections in humans difficult to cure (Drury et al., 2013; Frieri et al., 2017; Medernach and Logan, 2018). The World Health Organization studied the exact size of the world's bacterial resistance status in 2014 and reported that the resistance of common bacteria to antibiotics has reached alarming levels, and in several countries, the main groups of antibiotics have failed to benefit half of the patients (Organization, 2014). In addition, antibiotics may adversely affect human health by interfering with endocrines (Huang et al., 2018). Therefore, aqueous solution containing antibiotics must be effectively treated before being discharged into the environment. Tetracyclines have become one of the most consumed antibiotics in the world at low prices and broad-spectrum antibacterial properties (Zhang et al., 2018). The tetracycline residue in original wastewater of pharmaceutical factories was reported in extremely high levels (844–1077 mg · L⁻¹), while that in treated wastewater still ranged from several to dozens of mg · L⁻¹ (Li et al., 2008; Zhang et al., 2018). Therefore, two typical tetracyclines, namely tetracycline hydrochloride (TC) and doxycycline (DC), were selected as target pollutants.

The main methods of removing antibiotics from water are biodegradation (Zhang et al., 2017), hydrolysis (Sarmah et al., 2006), photodegradation (Lu et al., 2018), and adsorption (Zeng et al., 2018; Liu et al., 2019). Among them, the adsorption method, which is the most efficient, economical, and environmentally friendly, has been widely used in the treatment of aqueous solution containing antibiotics. Finding an effective adsorbent is the key to expanding the application of this technology to antibiotic aqueous solution treatment. Biochar seems to be a promising adsorption material in pollutant treatment technologies, owing to its porous structure, complex surface, abundance of raw material, and economic benefits (Tan et al., 2015, 2016b; Liang et al., 2017; Zhang et al., 2019b). However, there is room to further improve the adsorption capacity of original biochar (Cai et al., 2018, 2019; Zhang et al., 2019a).

Nanoparticles of manganese oxide have been widely reported as an effective adsorbent (Song et al., 2014). Nano-scale MnO_x particles have a high specific surface area owing to their superior polycrystalline structure, as well as high adsorption performance (Wang et al., 2010; Xiao et al., 2010). However, nano-sized MnO_x particles easily agglomerate, thus limiting their practical application as adsorbents (Tyson et al., 2011; Li et al., 2017). In this study, a simple, low-cost method of loading MnO_x nanoparticles onto biochar was developed for preparing a new biochar composite that can be used to adsorb antibiotics in aqueous solution. This method not only solves the agglomeration

problem, but also improves the effectiveness of the nano-metal oxide MnO_x in aiding biochar for better pollutant removal.

The main objectives of this study included: (1) Preparation of a biochar-supported manganese dioxide composite; (2) Characterization of the prepared composite using scanning electron microscopy (SEM), Fourier transform infrared spectroscopy (FTIR), X-ray diffraction (XRD), and X-ray photoelectron spectroscopy (XPS); (3) Removal of TC and DC using the prepared composite under different experimental conditions; (4) Evaluation of the isotherms and kinetic laws of the adsorption process.

MATERIALS AND METHODS

Material Preparation

Preparation of Biochar

Rice husk, which is a common agricultural waste, was used as the biomass raw material in the preparation of biochar. The rice husk collected from the farm was rinsed with ultrapure water and air dried. Subsequently, it was completely dried in an oven at 60°C and grounded to a powder form. The rice husk powder was placed in a quartz boat and then heated in a quartz tube furnace (SK-1200°C, Tianjin Zhonghuan Experimental Furnace Co., Ltd., Tianjin, China). Both ends of the quartz tube were sealed, and the hose was connected. N₂ was passed through the furnace chamber at a flow rate of 400 mL · min⁻¹ from one end, and an inert atmosphere was maintained during the pyrolysis process. The volatile products generated during the pyrolysis of biomass were collected from the other end. The temperature was programmed to increase to 500°C at a rate of 7°C min⁻¹ and was maintained at the peak temperature for 2 h, which was the optimal preparation condition in preliminary study (Wu et al., 2016). Finally, the chamber was cooled to room temperature (25 ± 1°C) to obtain rice husk biochar.

Synthesis of Biochar-Supported Nano Manganese Dioxide Composite

A 4 mmol · L⁻¹ manganese chloride solution was prepared and then purified under N₂ (100 mL · min⁻¹) for 20 min to remove dissolved oxygen. One gram of the above-mentioned chaff biochar was added to 30 mL of a manganese chloride solution and stirred under N₂ atmosphere (100 mL · min⁻¹) for 1 h to form a biochar–Mn²⁺ mixture. This mixture was added dropwise to 20 mL of a solution containing potassium permanganate and sodium hydroxide while stirring at 250 r · min⁻¹ using a magnetic stirrer. The stirring was continued for 20 min to ensure a complete reaction. After aging for 24 h at room temperature (25 ± 1°C), the mixture was washed several times with ultrapure water until the pH was neutral. Finally, it was completely dried in an oven at 80°C. After grinding, it was made to pass through a 100-mesh sieve to obtain a biochar-supported nano manganese dioxide composite (BC/MnO₂).

Characterization Methods

The microstructure and morphology of the composites were studied using a QUANTA 250 FE-SEM (FEI, United States).

XRD patterns were acquired using a Bruker D8-Advance X-ray diffractometer (Bruker, Germany). The surface elements were determined using an ESCALAB 250Xi X-ray photoelectron spectrometer (Thermo Fisher Scientific, United States). A Fourier transform infrared spectrometer was used (NICOLET 5700; Thermo Nicolet Corporation, United States). The thermogravimetric (TG) curve of the material was measured in N₂ atmosphere by varying the temperature from room temperature (25 ± 1°C) to 1000°C (flux rate: 100 mL · min⁻¹; heating rate: 10°C · min⁻¹) using an SDT Q600 thermal analyzer (TA, United States). The Brunner–Emmet–Teller (BET) specific surface area of the material was measured using a Micromeritics 3Flex analyzer (Micromeritics Instrument Corporation, United States).

Adsorption Experiments

Effect of Adsorbent Dose on Adsorption

Various amounts of BC/MnO₂ (10, 20, 40, 80, 100, and 150 mg) were added to 25 mL of 5 mg · L⁻¹ TC and DC solutions (pH = 6.0). The resulting mixture was sealed using a plastic wrap and rotated in a constant-temperature shaker at a speed of 170 r · min⁻¹. The reaction temperature was set to 25°C, and the mixture was shaken for 24 h. Finally, a sample was taken for measurement.

Effect of pH on Adsorption

TC and DC solutions (both the concentrations were 5 mg · L⁻¹) with a pH value ranging from 2.0 to 10.0 were prepared. Subsequently, 0.1 g of BC/MnO₂ was added to 25 mL of the above solution. The mixture was sealed using a plastic wrap and rotated in the constant-temperature shaker at a speed of 170 r · min⁻¹. The reaction temperature was set to 25°C, and the mixture was shaken for 24 h. Finally, a sample was taken for measurement.

Effect of Initial Antibiotics Concentration and Adsorption Temperature

TC and DC solutions were prepared at a concentration ranging from 5 to 100 mg · L⁻¹ (pH = 6.0). At reaction temperatures of 25, 35, and 45°C, 0.1 g of BC/MnO₂ was taken and added to 25 mL of the above solutions. The mixture was then sealed using a plastic wrap and rotated in the constant-temperature shaker at a speed of 170 r · min⁻¹. The mixture was shaken for 24 h and sampled for measurement.

Effect of Reaction Time on Adsorption

The kinetic test interval was from 0 to 1440 min. BC/MnO₂ (0.1 g) was added to 25 mL of TC and DC solutions with a concentration of 50 mg · L⁻¹, with pH = 6.0. The mixture was

sealed using a plastic wrap, and the reaction temperature was set to 25°C. It was then shaken in the constant temperature shaker at a speed of 170 r · min⁻¹. Samples were taken for measurement at the corresponding time.

Detection Method

The residual antibiotics concentration in the solution was determined by UV spectrophotometry (Ma et al., 2018). The solutions were separated and filtered, and the residual concentration of TC and DC in the liquid was detected by UV spectrophotometer (UV-2550, Shimadzu, Japan) at 357 nm (Jing et al., 2014) and 346 nm (Xiong et al., 2019), respectively.

RESULTS AND DISCUSSION

Characterization

Table 1 lists the physical and chemical characteristics of BC/MnO₂. The elemental analysis shows that compared with the

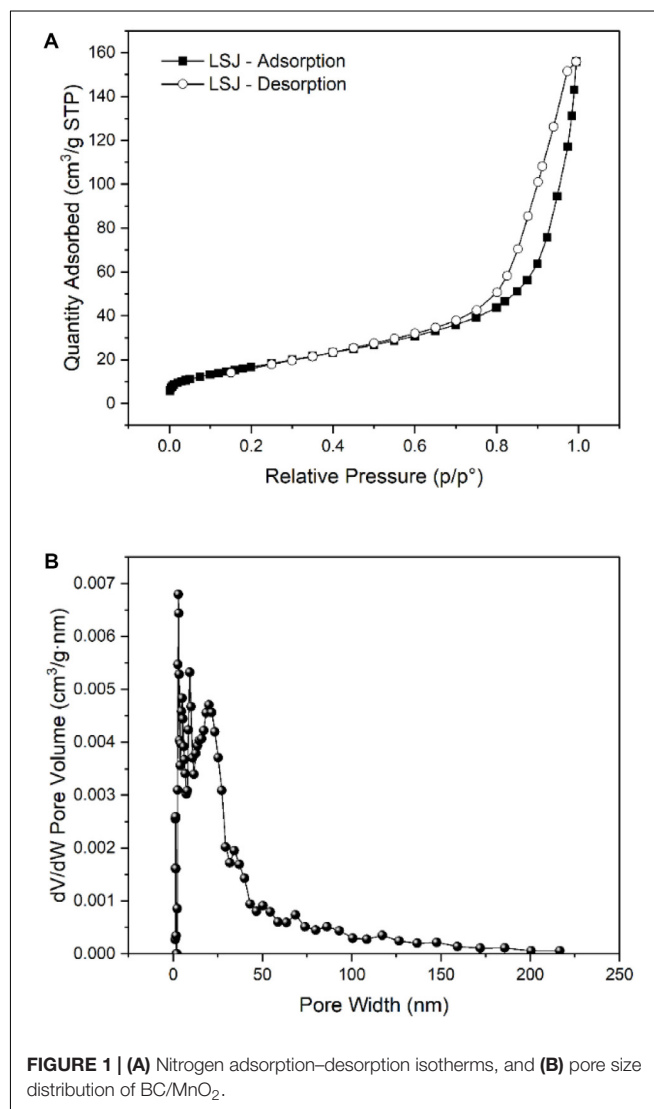


FIGURE 1 | (A) Nitrogen adsorption–desorption isotherms, and (B) pore size distribution of BC/MnO₂.

TABLE 1 | Characteristics of BC/MnO₂.

	BET surface area (m ² g ⁻¹)	Pore volume (cm ³ g ⁻¹)	Pore size (nm)	Bulk elemental composition (%)		
				C	O	Mn
BC	6.67	0.006	3.66	73.64	23.66	–
BC/MnO ₂	64.32	0.24	13.10	58.76	31.89	7.13

original biochar, manganese appears on the surface of BC/MnO₂ owing to the introduction of MnO₂, and the carbon content of the biochar is decreased, whereas the oxygen content is increased. Compared with the original biochar ($0.006 \text{ cm}^3 \cdot \text{g}^{-1}$), BC/MnO₂ ($0.24 \text{ cm}^3 \cdot \text{g}^{-1}$) has a significantly larger total pore volume. In addition, the specific surface area of the biochar is increased from 6.67 to $64.32 \text{ m}^2 \cdot \text{g}^{-1}$, indicating an improvement in its pore structure.

The N₂ adsorption-desorption isotherm and pore size distribution of BC/MnO₂ were measured at 77.3 K. **Figure 1** shows the results. According to the IUPAC classification, the shape of the isotherm is IV, indicating that BC/MnO₂ has a flat slit, wedge structure (Saiah et al., 2009). The pore size distribution of BC/MnO₂ is mainly in the range of 0–50 nm, and the average

pore size is 13.10 nm. The increased specific surface area and total pore volume were beneficial for improving the adsorption performance of BC/MnO₂.

Figure 2 shows the SEM morphologies of BC/MnO₂. BC/MnO₂ exhibits an irregular surface with micropores of different shapes and sizes, and a large number of particles are uniformly precipitated on the surface of biochar, indicating the successful coating of the MnO₂ nanoparticles on the biochar surface. The TEM image (**Figure 3**) shows that MnO₂ is successfully loaded on the biochar and that MnO₂ nano-flakes are embedded in the biochar matrix.

Figure 4A shows the XRD pattern of BC/MnO₂. The characteristic peak of BC/MnO₂ at $2\theta = 30.082^\circ$ indicates the presence of MnO₂ on the biochar surface. **Figure 4B** shows the

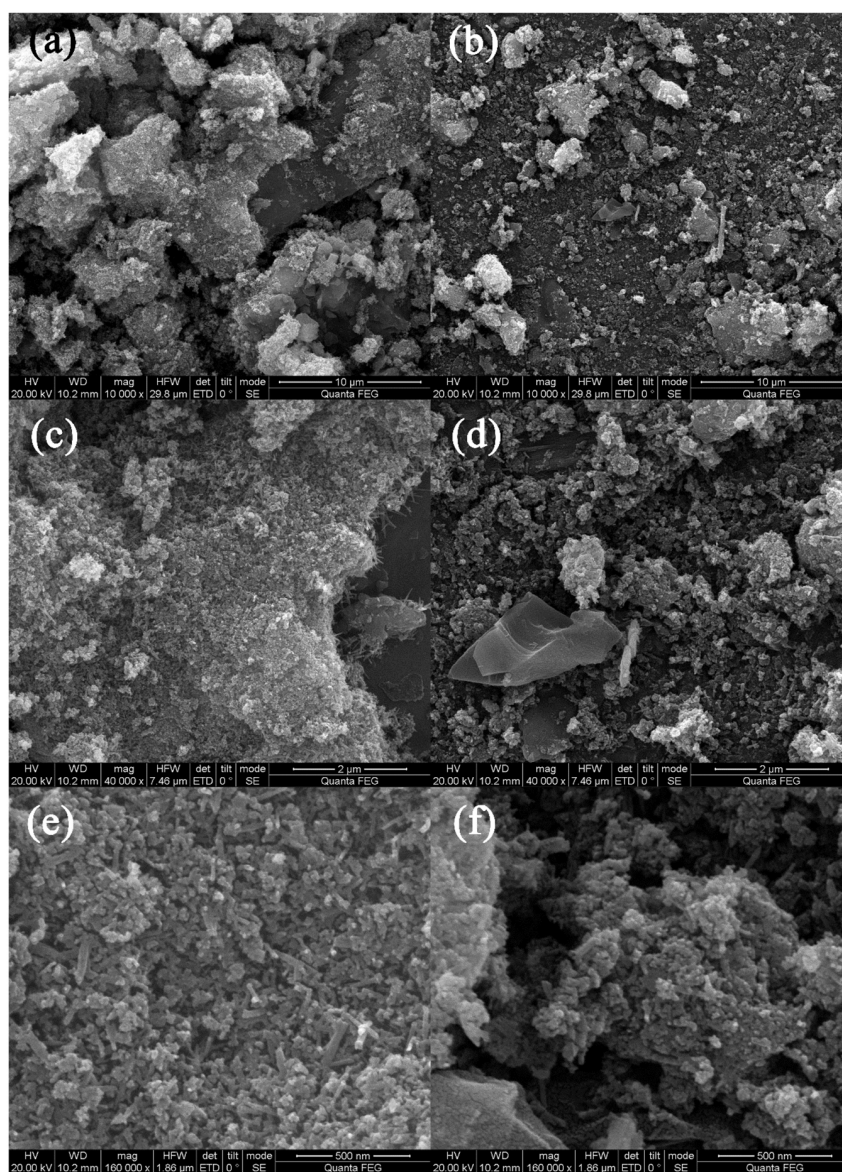
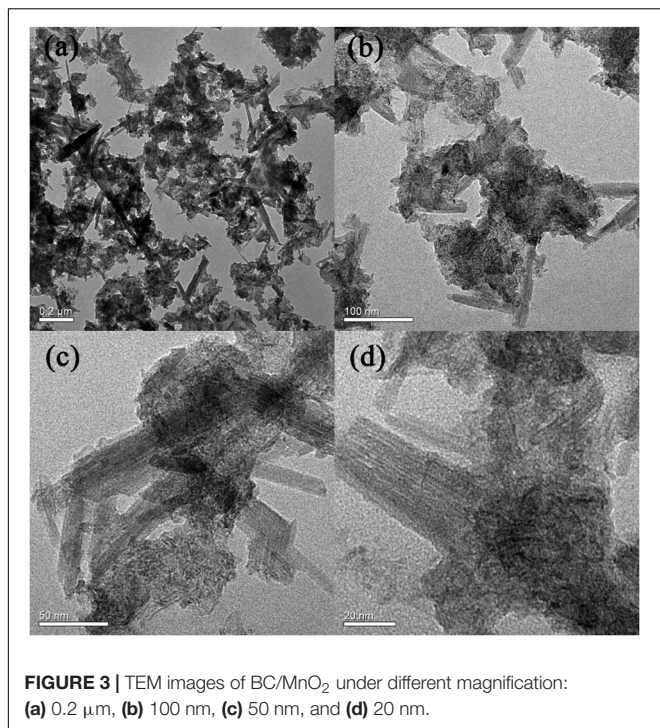


FIGURE 2 | SEM images of BC/MnO₂ under different magnification: (a,b) 10000 \times , (c,d) 40000 \times , and (e,f) 160000 \times .



TG analysis results. The weight loss of approximately 10% in the temperature range of 30–120°C is mainly due to the dehydration process (Shete et al., 2015). When the temperature gradually increases from 120 to 500°C, the weight loss of the biochar decreases by only approximately 20%. The weight loss at 800°C is approximately 30%. This shows that BC/MnO₂ has higher thermal stability than the original biochar.

The chemical composition of the BC/MnO₂ surface was further studied by conducting an XPS analysis (Figure 5). The characteristic Mn2p peak (Figure 5A) can be divided into three peaks by Gaussian fitting. The peak position of Mn⁴⁺ can be observed at 644.04 eV (Yin et al., 2015). The peaks at 642.05 and 653.78 eV belong to Mn2p_{3/2} and Mn2p_{1/2}, respectively,

with an energy interval of 11.73 eV, which is consistent with the results reported for MnO₂ (Xie et al., 2017; Li et al., 2018). The characteristic peaks of the XPS spectrum of O1s (Figure 5B) are 533.20, 531.55, 530.54, and 529.56 eV, indicating the presence of C-O, C = O, O-H, and Mn-O, respectively (Yu et al., 2007; Han et al., 2013; Zhang et al., 2014; Bose and Biju, 2015). These functional groups can serve as binding sites for the adsorption of antibiotics. The above results once again demonstrate the successful loading of the MnO₂ nanoparticles on the surface of biochar.

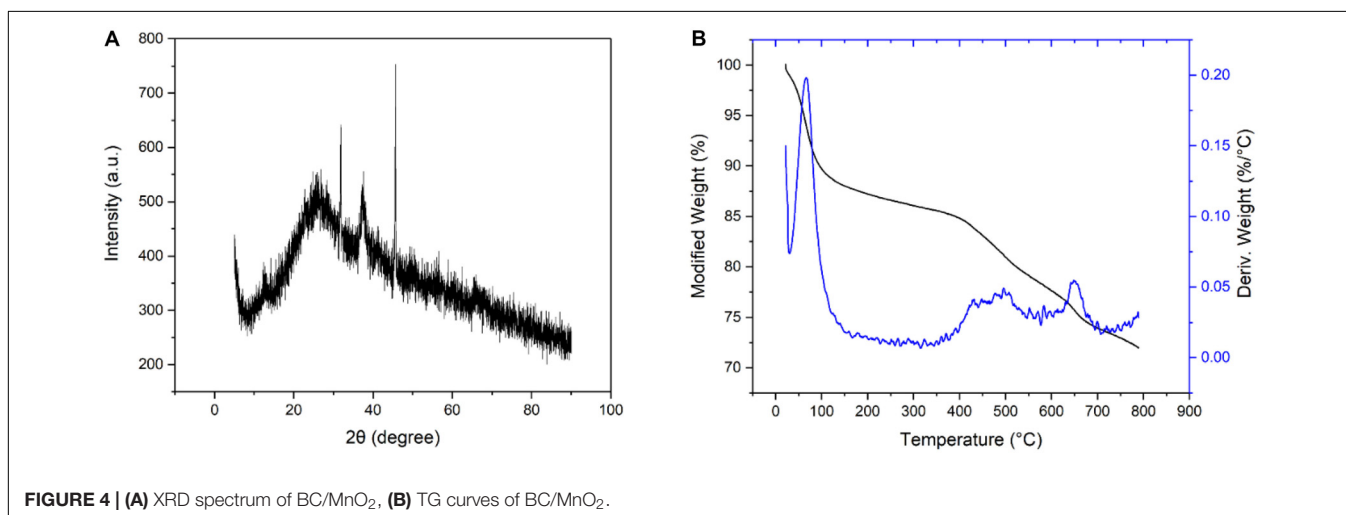
Comparison of the Performance of Pristine Biochar and BC/MnO₂

The adsorption ability of pristine biochar and BC/MnO₂ for TC and DC were compared at initial antibiotic concentrations range from 5 to 100 mg · L⁻¹. As can be seen from Figure 6, after the coating of MnO₂, the adsorption ability of BC/MnO₂ for both TC and DC were significantly higher than that of pristine biochar. These results suggested that the loading of MnO₂ was an effective way to improve the adsorption ability of biochar for TC and DC. The increased specific surface area and total pore volume, and the loading of MnO₂ served as bonding sites might be account for the enhanced adsorption performance of BC/MnO₂.

Effect of Adsorbent Dose

Figure 7 shows the effect of BC/MnO₂ dose on the adsorption of TC and DC. With the increase in the BC/MnO₂ dose, the relative adsorption amounts of TC and DC gradually decrease. This is mainly because an excessive dose leads to excess adsorption sites and reduces the adsorbent utilization rate (Wu et al., 2014). With the increase in the adsorbent dose, the removal rates of TC and DC increase, mainly because of the increase in the number of adsorption sites. However, there was no significant difference between the adsorption ability of BC/MnO₂ for TC and DC, with slightly higher performance for DC. Similar results could be found in the later adsorption experiments.

As can be seen from Figure 7, when the dose of BC/MnO₂ is 0.1 g, the effect of the composite material on antibiotic



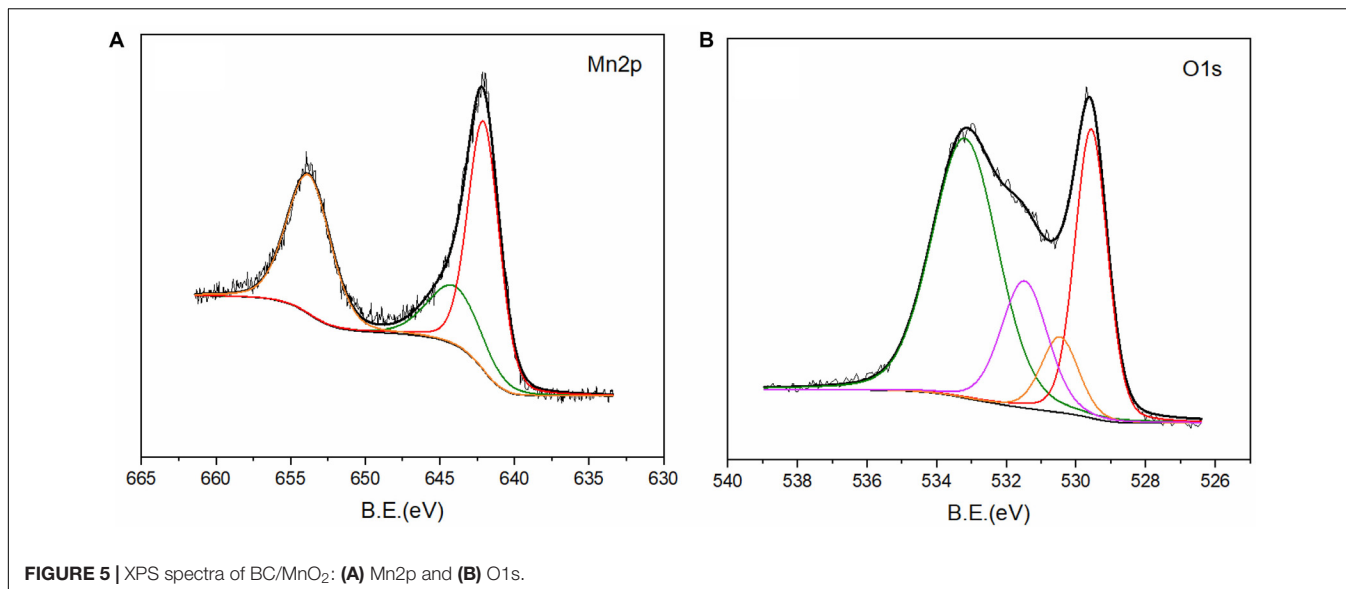


FIGURE 5 | XPS spectra of BC/MnO₂: (A) Mn2p and (B) O1s.

contaminants is very obvious, in which the removal rate of doxycycline reaches 90%, and the removal rate of tetracycline hydrochloride is nearly 95%. This is conducive to the comparative observation of experimental effects. Therefore, according to the concentration of antibiotic contaminants and the results of preliminary experiments, we chose 0.1 g as the dose of adsorbent in other parts of the experiment.

Effect of pH

Figure 8 shows the effect of initial pH on the adsorption of TC and DC by BC/MnO₂. According to the result obtained by **Figure 8B**, the zero-potential point of BC/MnO₂ is around 3.2. At low pH, TC and DC mainly exist in cationic form, and the surface of the biochar composite is positively charged (**Figure 8B**).

Therefore, under this condition, electrostatic repulsion may occur between them. Similarly, at high pH, anionic antibiotics are repelled by the negatively charged biochar surface (**Figure 8B**), inhibiting TC and DC adsorption (Wang et al., 2016). However, the removal rate did not change significantly across the tested pH range, suggesting that the electrostatic interactions were not the main mechanism whereby biochar composites adsorb TC and DC. Other forces may have formed between the antibiotics and the carboxyl or hydroxyl groups on the surface of the new biochar composite, including π - π interaction and hydrogen bonding (Zheng et al., 2013; Zeng et al., 2019; Ye et al., 2020). In addition, part of TC and DC could be adsorbed by MnO₂ particles on biochar surface (Mahamallik et al., 2015). Overall, the effect of pH on the adsorption of TC and DC by the new biochar composite is not significant.

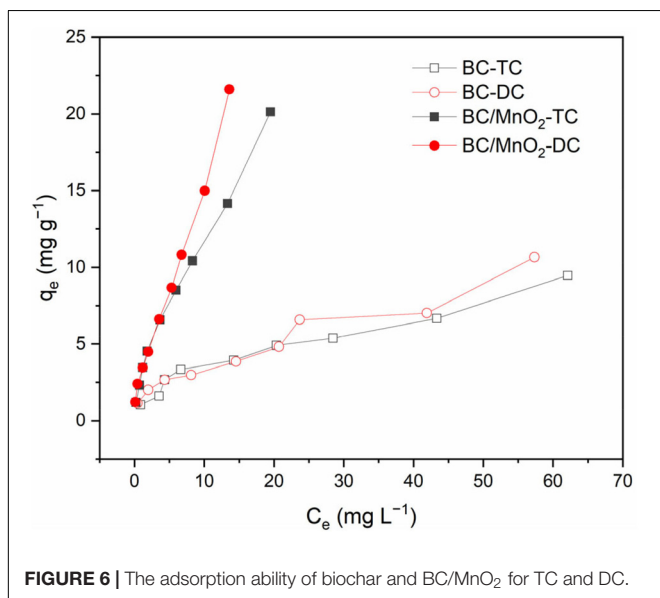


FIGURE 6 | The adsorption ability of biochar and BC/MnO₂ for TC and DC.

Adsorption Isotherms

The Langmuir, Freundlich and Temkin models were used to study the adsorption equilibrium isotherms and fit the experimental data. The adsorption models are expressed as follows (Zhang et al., 2019a):

$$\frac{C_e}{q_e} = \frac{C_e}{q_{\max}} + \frac{1}{q_{\max}K_L} \quad (1)$$

Here, q_e is the adsorption amount ($\text{mg} \cdot \text{g}^{-1}$); C_e is the concentration at the end of the adsorption reaction ($\text{mg} \cdot \text{L}^{-1}$); q_{\max} is the maximum adsorption amount ($\text{mg} \cdot \text{g}^{-1}$); and K_L is the Langmuir constant related to adsorption ($\text{L} \cdot \text{mg}^{-1}$), which is used to indicate whether the adsorption equilibrium is favorable ($0 < K_L < 1$) or unfavorable ($K_L > 1$).

$$\ln q_e = \ln K_F + \frac{1}{n} \ln C_e \quad (2)$$

Here, q_e is the adsorption amount ($\text{mg} \cdot \text{g}^{-1}$); C_e is the concentration at the end of the adsorption reaction ($\text{mg} \cdot \text{L}^{-1}$);

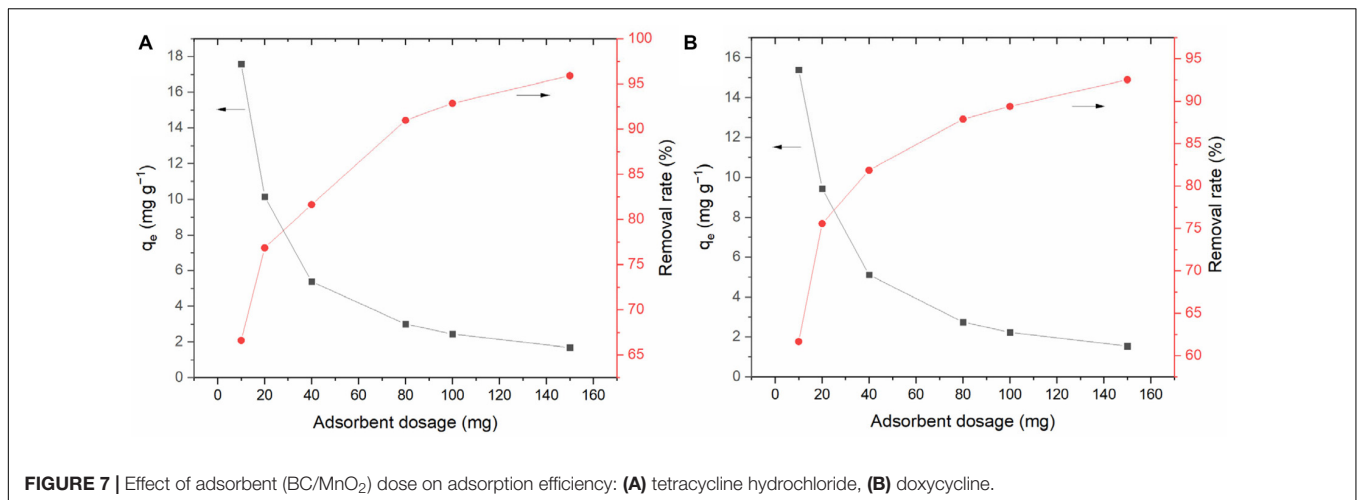


FIGURE 7 | Effect of adsorbent (BC/MnO₂) dose on adsorption efficiency: (A) tetracycline hydrochloride, (B) doxycycline.

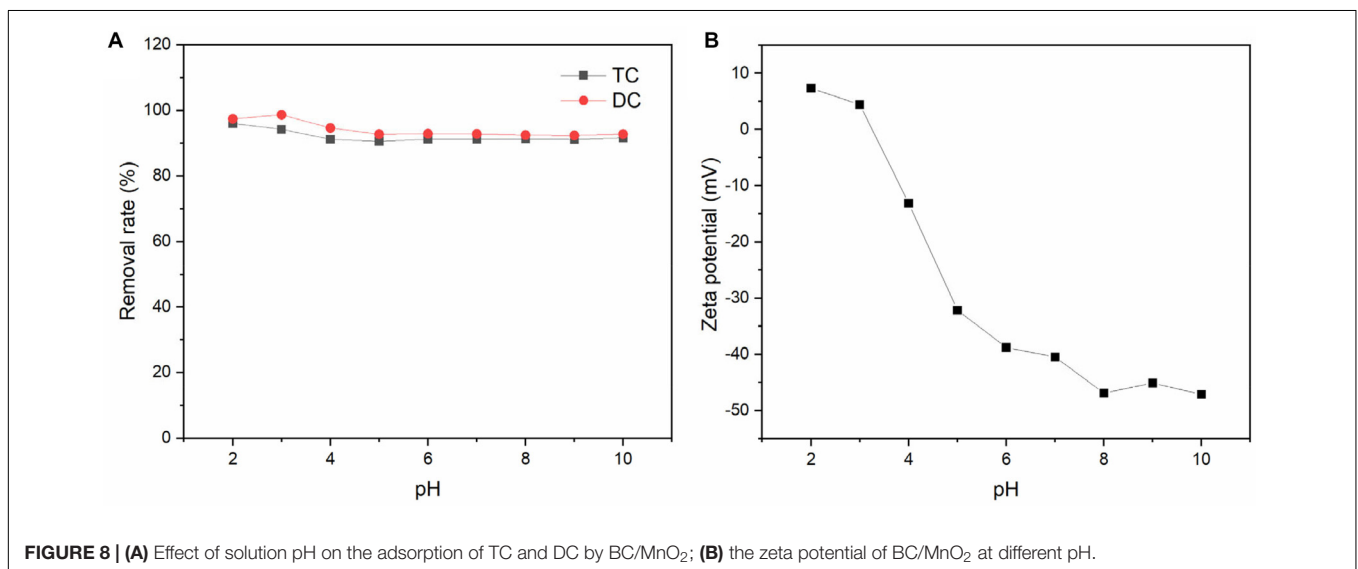


FIGURE 8 | (A) Effect of solution pH on the adsorption of TC and DC by BC/MnO₂; (B) the zeta potential of BC/MnO₂ at different pH.

K_F is the Freundlich constant ($\text{L} \cdot \text{mg}^{-1}$) representing the adsorption capacity; and n is the Freundlich constant representing the adsorption strength.

$$q_e = B_T \ln K_T + B_T \ln C_e \quad (3)$$

Here, q_e is the adsorption amount ($\text{mg} \cdot \text{g}^{-1}$), C_e is the concentration at the end of the adsorption reaction ($\text{mg} \cdot \text{L}^{-1}$). $B_T = RT/b_T$ and b_T ($\text{J} \cdot \text{mol}^{-1}$) is the Temkin constant, R is the universal gas constant ($8.314 \text{ J} \cdot \text{mol}^{-1} \cdot \text{K}^{-1}$) and T is the temperature (K); K_T ($\text{L} \cdot \text{mg}^{-1}$) is the maximum binding energy constant.

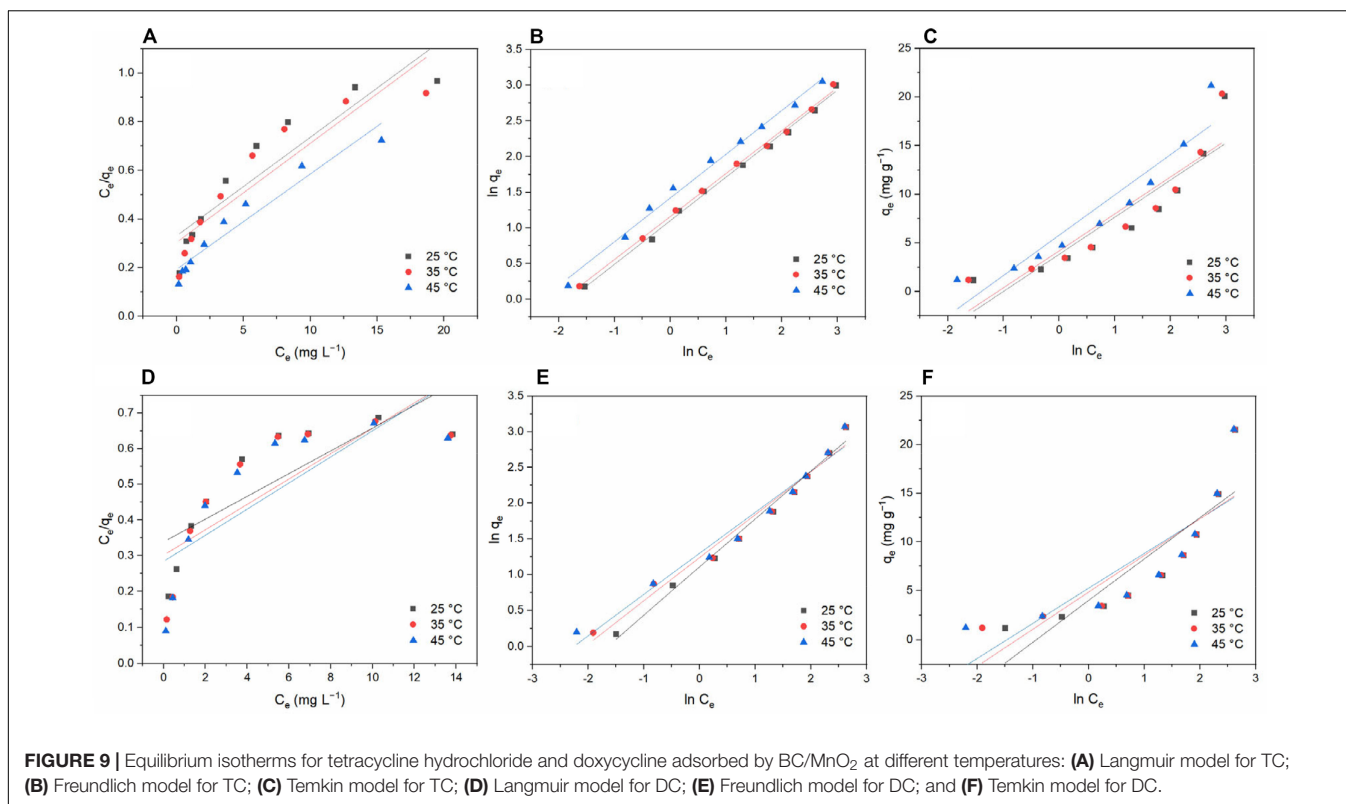
In the Langmuir model, it is assumed that a single molecular layer is formed when adsorption occurs and that the adsorbed molecules do not interact. Figure 9 shows the relationship between C_e/q_e and C_e . Table 2 lists the values of the related parameters. Temkin isotherm is based on an assumption that the indirect interactions are existed between adsorbate molecules, and the heat of adsorption of molecules will decrease linearly with surface coverage (Zhang et al., 2019a).

At the three temperatures studied, the adsorption data show a poor correlation with the Langmuir and Temkin model, whereas they show a strong correlation with the Freundlich model, indicating that the adsorption of TC and DC by BC/MnO₂ better conforms to the Freundlich adsorption model (Wu et al., 2014). The Freundlich adsorption model is an empirical equation where it is assumed that adsorption occurs on a heterogeneous surface and that the adsorption capacity is related to the equilibrium concentration (Cui et al., 2015). In Table 2, the values of $1/n$ are less than 1, indicating that TC and DC easily get adsorbed by BC/MnO₂ at these temperatures.

Thermodynamic analysis was further applied to study the adsorption process and mechanisms. The Gibbs free energy ΔG° , enthalpy ΔH° , entropy ΔS° were calculated using the following equations (Tan et al., 2016a):

$$\Delta G^0 = -RTK^0 \quad (4)$$

$$\ln k^0 = -\frac{\Delta H^0}{RT} + \frac{\Delta S^0}{R} \quad (5)$$



Here, R is the gas constant $8.314 \text{ J} \cdot \text{mol}^{-1} \cdot \text{K}^{-1}$, T (K) is the adsorption temperature; K^0 could be calculated by plotting $\ln(q_e/c_e)$ versus c_e and extrapolating c_e to zero.

TABLE 2 | Model parameters and the corresponding correlation coefficients of isotherm models.

Contaminants	Isotherms	Parameters	Temperature (K)		
			298	303	318
TC	Langmuir	q_{\max} (mg · g ⁻¹)	24.69	24.55	25.50
		K_L (L · mg ⁻¹)	0.12	0.13	0.20
		R^2	0.854	0.854	0.935
	Freundlich	$1/n$	0.61	0.60	0.61
		K_F (L · mg ⁻¹)	3.01	3.19	4.14
		R^2	0.997	0.997	0.993
	Temkin	K_t (L/mg)	2.74	3.02	4.06
		B_t	3.81	3.79	4.14
		R^2	0.810	0.809	0.848
DC	Langmuir	q_{\max} (mg · g ⁻¹)	650.28	675.65	638.61
		K_L (L · mg ⁻¹)	27.29	28.10	31.34
		R^2	0.649	0.640	0.662
	Freundlich	$1/n$	0.57	0.61	0.67
		K_F (L · mg ⁻¹)	3.66	3.45	3.03
		R^2	0.966	0.970	0.986
	Temkin	K_t (L · mg ⁻¹)	4.34	3.62	2.56
		B_t	3.57	3.77	4.25
		R^2	0.675	0.693	0.733
		b_t (J mol ⁻¹)	694.00	679.23	622.08

The calculated thermodynamic data of ΔG° , ΔH° , and ΔS° are given in **Table 3**. The negative value of ΔG° at three temperatures indicated the feasibility and spontaneous reaction of TC and DC adsorption onto BC/MnO₂. In addition, the ΔG° values of TC and DC decreased from -2.80 to $-4.25 \text{ kJ} \cdot \text{mol}^{-1}$ and from -3.33 to $-4.25 \text{ kJ} \cdot \text{mol}^{-1}$ with the increase of temperature, respectively, indicating that higher temperature was more favorable for adsorption. The positive ΔH° value indicated the endothermic property of the adsorption process. The positive value of ΔS° might be due to the increase of randomness of solid and solution interface in the process of adsorption (Tan et al., 2016a).

Adsorption Kinetics

To determine the adsorption equilibrium time of BC/MnO₂ for TC and DC and to study the kinetics of the adsorption process, the effect of time on the adsorption of TC and DC by BC/MnO₂ was analyzed. Two conventional kinetic models

TABLE 3 | Thermodynamic parameters for TC and DC adsorption by BC/MnO₂.

Contaminants	T (°C)	ΔG° (kJ mol ⁻¹)	ΔH° (kJ mol ⁻¹)	ΔS° (J mol ⁻¹ K)	R^2
TC	25	-2.80	13.76	46.93	0.892
	35	-3.13			
	45	-4.25			
DC	25	-3.33	7.06	26.08	0.977
	35	-3.69			
	45	-4.25			

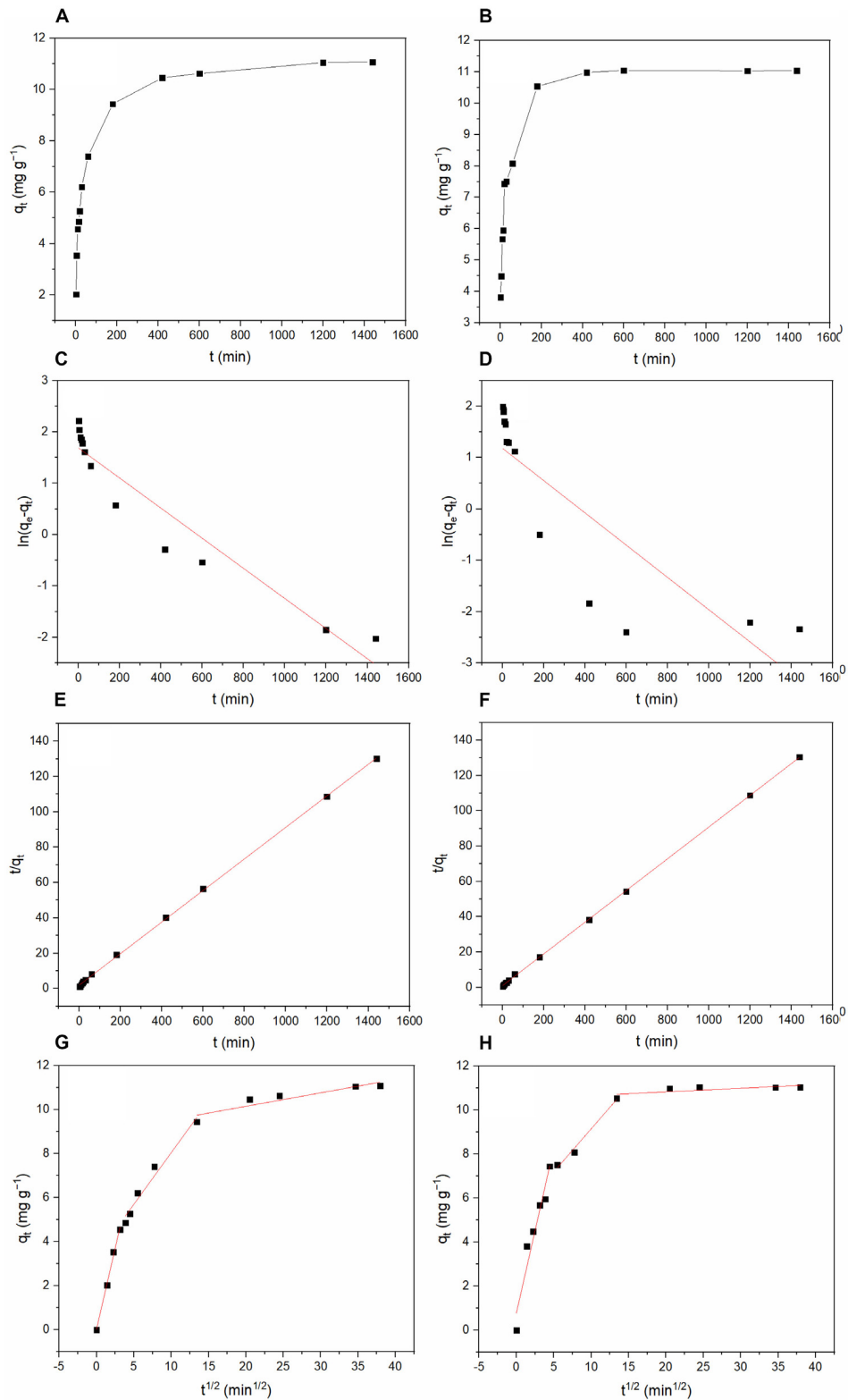


FIGURE 10 | Kinetics of the adsorption process of TC and DC by BC/MnO₂: **(A)** Change in TC adsorption amount with time; **(B)** Change in DC adsorption amount with time; **(C)** TC adsorption modeled using the pseudo-first-order equation; **(D)** DC adsorption modeled using the pseudo-first-order equation; **(E)** TC adsorption modeled using the pseudo-second-order equation; **(F)** DC adsorption modeled using the pseudo-second-order equation; **(G)** TC adsorption modeled using Intraparticle diffusion equation; and **(H)** DC adsorption modeled using Intraparticle diffusion equation.

were used to analyze the results: a pseudo-first-order kinetic model and a pseudo-second-order kinetic model. Intra-particle diffusion model was further applied to determine the diffusion mechanisms and the rate controlling procedures.

The pseudo-first-level model is expressed as:

$$\ln(q_e - q_t) = \ln q_e - k_1 t \quad (6)$$

The pseudo-secondary model is expressed as:

$$\frac{t}{q_t} = \frac{1}{k_2 q_e^2} + \frac{t}{q_e} \quad (7)$$

Here, q_e is the removal amount at equilibrium ($\text{mg} \cdot \text{g}^{-1}$); q_t is the removal amount at a given time t ($\text{mg} \cdot \text{g}^{-1}$); k_1 is the adsorption rate constant of the pseudo-first-order model (min^{-1}); and k_2 is the adsorption rate constant of the pseudo-second-order model ($\text{g} \cdot \text{mg}^{-1} \cdot \text{min}^{-1}$).

The intra-particle diffusion model is expressed as Zeng et al. (2018):

$$q_t = k_{id} t^{1/2} + c_i \quad (8)$$

Here, q_t ($\text{mg} \cdot \text{g}^{-1}$) is the removal amount at time t , k_{id} is the intra-particle diffusion rate constant ($\text{mg} \cdot \text{g}^{-1} \cdot \text{min}^{-1/2}$), and c_i is the intercept related to the thickness of the boundary layer.

Figure 10 shows the results of the adsorption kinetics study. **Table 4** lists the parameter values. The adsorption process reached equilibrium after 420 min. Compared with the pseudo-first-order kinetic model, the adsorption data better fit the pseudo-second-order kinetic model ($R^2 = 0.999$) (Turki et al., 2015). The pseudo-second-order kinetic model fitting results indicate that the process controlling the adsorption of TC and DC may be chemisorption (Tan et al., 2015). As shown in **Figure 10** and **Table 5**, three linear portions were existed in the plots of q_t against $t^{1/2}$, suggesting that multiple steps including intra-particle diffusion and film diffusion were involved in the adsorption process.

Regeneration of BC/MnO₂

To investigate the regeneration ability of BC/MnO₂, several cycles of adsorption-desorption experiments were performed.

TABLE 4 | Model parameters and corresponding correlation coefficients of kinetics models.

Contaminants	Kinetics	Parameters	
TC	Pseudo-first-order	q_e ($\text{mg} \cdot \text{g}^{-1}$)	5.41
		K_1 (min^{-1})	0.0029
		R^2	0.924
	Pseudo-second-order	q_e ($\text{mg} \cdot \text{g}^{-1}$)	11.20
		K_2 ($\text{g} \cdot \text{mg}^{-1} \cdot \text{min}^{-1}$)	0.0041
		R^2	0.999
DC	Pseudo-first-order	q_e ($\text{mg} \cdot \text{g}^{-1}$)	3.25
		K_1 (min^{-1})	0.0031
		R^2	0.732
	Pseudo-second-order	q_e ($\text{mg} \cdot \text{g}^{-1}$)	11.14
		K_2 ($\text{g} \cdot \text{mg}^{-1} \cdot \text{min}^{-1}$)	0.0085
		R^2	0.999

TABLE 5 | Intra-particle diffusion parameters for the adsorption of TC and DC by BC/MnO₂.

Contaminants	k_{id} ($\text{mg} \cdot \text{g}^{-1} \cdot \text{min}^{-0.5}$)	c_i	R_i^2
TC			
Section1	1.47	0.02	0.997
Section2	0.47	3.35	0.984
Section3	0.06	8.92	0.929
DC			
Section1	1.50	0.78	0.969
Section2	0.39	5.23	0.995
Section3	0.02	10.49	0.754

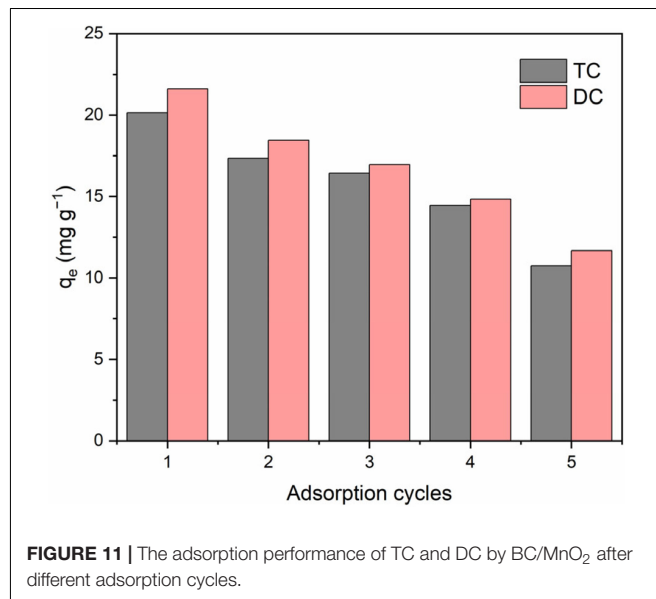


FIGURE 11 | The adsorption performance of TC and DC by BC/MnO₂ after different adsorption cycles.

The TC and DC loaded BC/MnO₂ was desorbed using ethanol. The adsorption performance of TC and DC by BC/MnO₂ after different adsorption cycles are shown in **Figure 11**. The results indicated that the adsorption capacity of BC/MnO₂ decreased gradually with the increase of cycles. After five adsorption/desorption cycles, the adsorption amount of TC and DC onto the regenerated BC/MnO₂ still remained higher than the pristine biochar, indicating that BC/MnO₂ could be regenerated.

CONCLUSION

In this study, a biochar-supported nano manganese dioxide composite was prepared by loading manganese dioxide nanoparticles on biochar, with rice husk as the raw material. Compared with the original biochar, MnO₂ nanoparticles appeared on the surface of BC/MnO₂, the carbon content decreased, and the oxygen content increased. BC/MnO₂ exhibited significantly larger total pore volume and specific surface area, and the pore structure of the biochar was improved. The comparative study about the adsorption ability of pristine biochar and BC/MnO₂ suggested that the loading of MnO₂ was

an effective way to improve the adsorption ability of biochar for TC and DC. The effects of pH on the adsorption of TC and DC by BC/MnO₂ were found to be insignificant. With an increase in the adsorbent dose, the removal rates of TC and DC increased, and the removal ability of BC/MnO₂ for TC was slightly higher than that for DC. Therefore, BC/MnO₂ may be an efficient material for TC and DC removal from aqueous solution. Further research about its efficiency for other antibiotics removal and deeper mechanisms should be studied.

DATA AVAILABILITY STATEMENT

The datasets generated for this study are available on request to the corresponding author.

REFERENCES

- Ahmed, M. B., Zhou, J. L., Ngo, H. H., and Guo, W. (2015). Adsorptive removal of antibiotics from water and wastewater: Progress and challenges. *Sci. Total Environ.* 532, 112–126. doi: 10.1016/j.scitotenv.2015.05.130
- Bose, V. C., and Biju, V. (2015). Mixed valence nanostructured Mn₃O₄ for supercapacitor applications. *Bull. Mater. Sci.* 38, 865–873. doi: 10.1007/s12034-015-0906-z
- Cai, X., Li, J., Liu, Y., Hu, X., Tan, X., Liu, S., et al. (2019). Design and preparation of chitosan-crosslinked bismuth ferrite/biochar coupled magnetic material for methylene blue removal. *Int. J. Environ. Res. Public Health* 17:6. doi: 10.3390/ijerph17010006
- Cai, X., Li, J., Liu, Y., Yan, Z., Tan, X., Liu, S., et al. (2018). Titanium dioxide-coated biochar composites as adsorptive and photocatalytic degradation materials for the removal of aqueous organic pollutants. *J. Chem. Technol. Biotechnol.* 93, 783–791. doi: 10.1002/jctb.5428
- Carvalho, I. T., and Santos, L. (2016). Antibiotics in the aquatic environments: a review of the European scenario. *Environ. Int.* 94, 736–757. doi: 10.1016/j.envint.2016.06.025
- Cui, L., Wang, Y., Gao, L., Hu, L., Yan, L., Wei, Q., et al. (2015). EDTA functionalized magnetic graphene oxide for removal of Pb(II), Hg(II) and Cu(II) in water treatment: adsorption mechanism and separation property. *Chem. Eng. J.* 281, 1–10. doi: 10.1016/j.cej.2015.06.043
- Drury, B., Scott, J., Rosi-Marshall, E. J., and Kelly, J. J. (2013). Triclosan exposure increases triclosan resistance and influences taxonomic composition of benthic bacterial communities. *Environ. Sci. Technol.* 47, 8923–8930. doi: 10.1021/es401919k
- Frieri, M., Kumar, K., and Boutin, A. (2017). Antibiotic resistance. *J. Infect. Public Health* 10, 369–378. doi: 10.1016/j.jiph.2016.08.007
- Han, H. S., You, J.-M., Jeong, H., and Jeon, S. (2013). Synthesis of graphene oxide grafted poly(lactic acid) with palladium nanoparticles and its application to serotonin sensing. *Appl. Surf. Sci.* 284, 438–445. doi: 10.1016/j.apsusc.2013.07.116
- Homem, V., and Santos, L. (2011). Degradation and removal methods of antibiotics from aqueous matrices – A review. *J. Environ. Manage.* 92, 2304–2347. doi: 10.1016/j.jenvman.2011.05.023
- Hong, P., Al-Jassim, N., Ansari, I. M., and Mackie, I. R. (2013). Environmental and public health implications of water reuse: antibiotics, antibiotic resistant bacteria, and antibiotic resistance genes. *Antibiotics* 2, 367–399. doi: 10.3390/antibiotics2030367
- Hou, J., Wang, C., Mao, D., and Luo, Y. (2016). The occurrence and fate of tetracyclines in two pharmaceutical wastewater treatment plants of Northern China. *Environ. Sci. Pollut. Res.* 23, 1722–1731. doi: 10.1007/s11356-015-5431-5
- Huang, D., Guo, X., Peng, Z., Zeng, G., Xu, P., Gong, X., et al. (2018). White rot fungi and advanced combined biotechnology with nanomaterials: promising tools for endocrine-disrupting compounds biotransformation. *Crit. Rev. Biotechnol.* 38, 671–689. doi: 10.1080/07388551.2017.1386613

AUTHOR CONTRIBUTIONS

JL and XC contributed conception and design of the study. YL and YG organized the database. HW, ShaL, SimL, YY, and SijL performed the statistical analysis. All authors contributed to manuscript revision, read and approved the submitted version.

FUNDING

This study was financially supported by the National Natural Science Foundation of China (Grant No. 51909283) and the Natural Science Foundation of Hunan Province, China (Grant No. 2018JJ3096).

- Huang, X., Liu, C., Li, K., Su, J., Zhu, G., and Liu, L. (2015). Performance of vertical up-flow constructed wetlands on swine wastewater containing tetracyclines and tet genes. *Water Res.* 70, 109–117. doi: 10.1016/j.watres.2014.11.048
- Jing, X., Wang, Y., Liu, W., Wang, Y., and Jiang, H. (2014). Enhanced adsorption performance of tetracycline in aqueous solutions by methanol-modified biochar. *Chem. Eng. J.* 248, 168–174. doi: 10.1016/j.cej.2014.03.006
- Kasprzyk-Hordern, B., Dinsdale, R. M., and Guwy, A. J. (2009). The removal of pharmaceuticals, personal care products, endocrine disruptors and illicit drugs during wastewater treatment and its impact on the quality of receiving waters. *Water Res.* 43, 363–380. doi: 10.1016/j.watres.2008.10.047
- Li, H., Huang, G., Zhang, J., Fu, S., Wang, T., and Liao, H. (2017). Photochemical synthesis and enhanced photocatalytic activity of MnOx/BiPO₄ heterojunction. *Trans. Nonferrous Met. Soc. China* 27, 1127–1133. doi: 10.1016/S1003-6326(17)60131-6
- Li, K., Yediler, A., Yang, M., Schulte-Hostede, S., and Wong, M. H. (2008). Ozonation of oxytetracycline and toxicological assessment of its oxidation by-products. *Chemosphere* 72, 473–478. doi: 10.1016/j.chemosphere.2008.02.008
- Li, R., Yu, L., Li, S., Fan, J., Luo, R., and Zhao, J. (2018). Facile synthesis of hierarchical mesoporous beta-manganese dioxide nanoflowers with extremely high specific surface areas for high-performance electrochemical capacitors. *Electrochim. Acta* 284, 52–59. doi: 10.1016/j.electacta.2018.07.172
- Liang, J., Li, X., Yu, Z., Zeng, G., Luo, Y., Jiang, L., et al. (2017). Amorphous MnO₂ modified biochar derived from aerobically composted swine manure for adsorption of Pb(II) and Cd(II). *ACS Sustainable Chem. Eng.* 5, 5049–5058. doi: 10.1021/acsschemeng.7b00434
- Liu, S., Liu, Y., Tan, X., Liu, S., Li, M., Liu, N., et al. (2019). Facile synthesis of MnOx-loaded biochar for the removal of doxycycline hydrochloride: effects of ambient conditions and co-existing heavy metals. *J. Chem. Technol. Biotechnol.* 94, 2187–2197. doi: 10.1002/jctb.6000
- Lu, X., Wang, Y., Zhang, X., Xu, G., Wang, D., Lv, J., et al. (2018). NiS and MoS₂ nanosheet co-modified graphitic C₃N₄ ternary heterostructure for high efficient visible light photodegradation of antibiotic. *J. Hazard. Mater.* 341, 10–19. doi: 10.1016/j.jhazmat.2017.07.004
- Luo, Y., Xu, L., Rysz, M., Wang, Y., Zhang, H., and Alvarez, P. J. J. (2011). Occurrence and transport of tetracycline, sulfonamide, quinolone, and macrolide antibiotics in the Haihe River Basin, China. *Environ. Sci. Technol.* 45, 1827–1833. doi: 10.1021/es104009s
- Ma, C., Huang, H., Gao, X., Wang, T., Zhu, Z., Huo, P., et al. (2018). Honeycomb tubular biochar from fargesia leaves as an effective adsorbent for tetracyclines pollutants. *J. Taiwan Inst. Chem. Eng.* 91, 299–308. doi: 10.1016/j.jtice.2018.05.032
- Mahamallik, P., Saha, S., and Pal, A. (2015). Tetracycline degradation in aquatic environment by highly porous MnO₂ nanosheet assembly. *Chem. Eng. J.* 276, 155–165. doi: 10.1016/j.cej.2015.04.064
- Medernach, R. L., and Logan, L. K. (2018). The growing threat of antibiotic resistance in children. *Infect. Dis. Clin.* 32, 1–17. doi: 10.1016/j.idc.2017.11.001

- Organization, W. H. (2014). *Antimicrobial Resistance: Global Report on Surveillance*. Geneva: World Health Organization.
- Petrie, B., Barden, R., and Kasprzyk-Hordern, B. (2015). A review on emerging contaminants in wastewaters and the environment: Current knowledge, understudied areas and recommendations for future monitoring. *Water Res.* 72, 3–27. doi: 10.1016/j.watres.2014.08.053
- Saiah, F. B. D., Su, B.-L., and Bettahar, N. (2009). Nickel-iron layered double hydroxide (LDH): Textural properties upon hydrothermal treatments and application on dye sorption. *J. Hazard. Mater.* 165, 206–217. doi: 10.1016/j.jhazmat.2008.09.125
- Sarmah, A. K., Meyer, M. T., and Boxall, A. B. A. (2006). A global perspective on the use, sales, exposure pathways, occurrence, fate and effects of veterinary antibiotics (VAs) in the environment. *Chemosphere* 65, 725–759. doi: 10.1016/j.chemosphere.2006.03.026
- Sharma, V. K., Johnson, N., Cizmas, L., McDonald, T. J., and Kim, H. (2016). A review of the influence of treatment strategies on antibiotic resistant bacteria and antibiotic resistance genes. *Chemosphere* 150, 702–714. doi: 10.1016/j.chemosphere.2015.12.084
- Shete, P. B., Patil, R. M., Tiwale, B. M., and Pawar, S. H. (2015). Water dispersible oleic acid-coated Fe₃O₄ nanoparticles for biomedical applications. *J. Magn. Mater.* 377, 406–410. doi: 10.1016/j.jmmm.2014.10.137
- Song, Z., Lian, F., Yu, Z., Zhu, L., Xing, B., and Qiu, W. (2014). Synthesis and characterization of a novel MnOx-loaded biochar and its adsorption properties for Cu²⁺ in aqueous solution. *Chem. Eng. J.* 242, 36–42. doi: 10.1016/j.cej.2013.12.061
- Tan, X., Liu, S., Liu, Y., Gu, Y., Zeng, G., Cai, X., et al. (2016a). One-pot synthesis of carbon supported calcined-Mg/Al layered double hydroxides for antibiotic removal by slow pyrolysis of biomass waste. *Sci. Rep.* 6:39691. doi: 10.1038/srep39691
- Tan, X., Liu, Y., Gu, Y., Xu, Y., Zeng, G., Hu, X., et al. (2016b). Biochar-based nanocomposites for the decontamination of wastewater: a review. *Bioresour. Technol.* 212, 318–333. doi: 10.1016/j.biortech.2016.04.093
- Tan, X., Liu, Y., Zeng, G., Wang, X., Hu, X., Gu, Y., et al. (2015). Application of biochar for the removal of pollutants from aqueous solutions. *Chemosphere* 125, 70–85. doi: 10.1016/j.chemosphere.2014.12.058
- Turki, A., Guillard, C., Dappozze, F., Ksibi, Z., Berhault, G., and Kochkar, H. (2015). Phenol photocatalytic degradation over anisotropic TiO₂ nanomaterials: Kinetic study, adsorption isotherms and formal mechanisms. *Appl. Catal. B Environ.* 163, 404–414. doi: 10.1016/j.apcatb.2014.08.010
- Tyson, B. M., Abu Al-Rub, R. K., Yazdanbakhsh, A., and Grasley, Z. (2011). A quantitative method for analyzing the dispersion and agglomeration of nanoparticles in composite materials. *Compos. Pt. B Eng.* 42, 1395–1403. doi: 10.1016/j.compositesb.2011.05.020
- Wang, H., Yuan, X., Wu, Y., Zeng, G., Dong, H., Chen, X., et al. (2016). In situ synthesis of In₂S₃@MIL-125(Ti) core-shell microparticle for the removal of tetracycline from wastewater by integrated adsorption and visible-light-driven photocatalysis. *Appl. Catal. B Environ.* 186, 19–29. doi: 10.1016/j.apcatb.2015.12.041
- Wang, S., Xiao, L., Fang, Z., Qiu, G., and Wang, C. (2010). Electrogenative leaching for sphalerite-MnO₂ in the presence of *Acidithiobacillus thiooxidans*. *Trans. Nonferrous Met. Soc. China* 20, s21–s25. doi: 10.1016/S1003-6326(10)60005-2
- Wu, Y., Zhang, P., Zhang, H., Zeng, G., Liu, J., Ye, J., et al. (2016). Possibility of sludge conditioning and dewatering with rice husk biochar modified by ferric chloride. *Bioresour. Technol.* 205, 258–263. doi: 10.1016/j.biortech.2016.01.020
- Wu, Z., Zhong, H., Yuan, X., Wang, H., Wang, L., Chen, X., et al. (2014). Adsorptive removal of methylene blue by rhamnolipid-functionalized graphene oxide from wastewater. *Water Res.* 67, 330–344. doi: 10.1016/j.watres.2014.09.026
- Xiao, L., Fang, Z., Qiu, G., Wang, S., and Wang, C. (2010). Mechanism of electrogenerative-leaching of chalcopyrite-MnO₂ in presence of *Acidithiobacillus ferrooxidans*. *Trans. Nonferrous Met. Soc. China* 20, s15–s20. doi: 10.1016/S1003-6326(10)60004-0
- Xie, G., Liu, X., Li, Q., Lin, H., Li, Y., Nie, M., et al. (2017). The evolution of α-MnO₂ from hollow cubes to hollow spheres and their electrochemical performance for supercapacitors. *J. Mater. Sci.* 52, 10915–10926. doi: 10.1007/s10853-017-1116-4
- Xiong, W., Zeng, Z., Li, X., Zeng, G., Xiao, R., Yang, Z., et al. (2019). Ni-doped MIL-53(Fe) nanoparticles for optimized doxycycline removal by using response surface methodology from aqueous solution. *Chemosphere* 232, 186–194. doi: 10.1016/j.chemosphere.2019.05.184
- Ye, S., Zeng, G., Tan, X., Wu, H., Liang, J., Song, B., et al. (2020). Nitrogen-doped biochar fiber with graphitization from *Boehmeria nivea* for promoted peroxymonosulfate activation and non-radical degradation pathways with enhancing electron transfer. *Appl. Catal. B Environ.* 269:118850. doi: 10.1016/j.apcatb.2020.118850
- Yin, X., Liu, X., Zhan, Y., Zhang, H., and Chen, Q. (2015). Effect of Ag addition on the magnetic and electrical properties of La_{0.67}Ca_{0.33}MnO₃ films. *Appl. Surf. Sci.* 349, 983–987. doi: 10.1016/j.apsusc.2015.04.218
- Yu, F., Li, Y., Han, S., and Ma, J. (2016). Adsorptive removal of antibiotics from aqueous solution using carbon materials. *Chemosphere* 153, 365–385. doi: 10.1016/j.chemosphere.2016.03.083
- Yu, J., Tong, M., Sun, X., and Li, B. (2007). A simple method to prepare poly(amic acid)-modified biomass for enhancement of lead and cadmium adsorption. *Biochem. Eng. J.* 33, 126–133. doi: 10.1016/j.bej.2006.10.012
- Zeng, Z., Tan, X., Liu, Y., Tian, S., Zeng, G., Jiang, L., et al. (2018). Comprehensive adsorption studies of doxycycline and ciprofloxacin antibiotics by biochars prepared at different temperatures. *Front. Chem.* 6:80. doi: 10.3389/fchem.2018.00080
- Zeng, Z., Ye, S., Wu, H., Xiao, R., Zeng, G., Liang, J., et al. (2019). Research on the sustainable efficacy of g-MoS₂ decorated biochar nanocomposites for removing tetracycline hydrochloride from antibiotic-polluted aqueous solution. *Sci. Total Environ.* 648, 206–217. doi: 10.1016/j.scitotenv.2018.08.108
- Zhang, P., Liu, S., Tan, X., Liu, Y., Zeng, G., Yin, Z., et al. (2019a). Microwave-assisted chemical modification method for surface regulation of biochar and its application for estrogen removal. *Process Saf. Environ. Prot.* 128, 329–341. doi: 10.1016/j.psep.2019.06.009
- Zhang, P., Tan, X., Liu, S., Liu, Y., Zeng, G., Ye, S., et al. (2019b). Catalytic degradation of estrogen by persulfate activated with iron-doped graphitic biochar: Process variables effects and matrix effects. *Chem. Eng. J.* 378:122141. doi: 10.1016/j.cej.2019.122141
- Zhang, Y., Hu, S., Zhang, H., Shen, G., Yuan, Z., and Zhang, W. (2017). Degradation kinetics and mechanism of sulfadiazine and sulfamethoxazole in an agricultural soil system with manure application. *Sci. Total Environ.* 607–608, 1348–1356. doi: 10.1016/j.scitotenv.2017.07.083
- Zhang, Y., Xing, Z., Duan, Z., Meng, L., and Wang, Y. (2014). Effects of steam activation on the pore structure and surface chemistry of activated carbon derived from bamboo waste. *Appl. Surf. Sci.* 315, 279–286. doi: 10.1016/j.apsusc.2014.07.126
- Zhang, Z., Gao, P., Cheng, J., Liu, G., Zhang, X., and Feng, Y. (2018). Enhancing anaerobic digestion and methane production of tetracycline wastewater in EGSB reactor with GAC/NZVI mediator. *Water Res.* 136, 54–63. doi: 10.1016/j.watres.2018.02.025
- Zheng, H., Wang, Z., Zhao, J., Herbert, S., and Xing, B. (2013). Sorption of antibiotic sulfamethoxazole varies with biochars produced at different temperatures. *Environ. Pollut.* 181, 60–67. doi: 10.1016/j.envpol.2013.05.056

Conflict of Interest: The authors declare that the research was conducted in the absence of any commercial or financial relationships that could be construed as a potential conflict of interest.

Copyright © 2020 Li, Cai, Liu, Gu, Wang, Liu, Liu, Yin and Liu. This is an open-access article distributed under the terms of the Creative Commons Attribution License (CC BY). The use, distribution or reproduction in other forums is permitted, provided the original author(s) and the copyright owner(s) are credited and that the original publication in this journal is cited, in accordance with accepted academic practice. No use, distribution or reproduction is permitted which does not comply with these terms.